PHYSICAL REVIEW D **88,** 064041 (2013)

Geodesics in the linearized multipole solution: Distinguishing black holes from naked singularities

J. L. Hernandez-Pastora*

Departamento de Matematica Aplicada and Instituto Universitario de Fisica Fundamental y Matematicas, Universidad de Salamanca, Salamanca 37007, Spain

L. Herrera†

Departamento de Física Teórica e Historia de la Ciencia, Universidad del País Vasco, Bilbao 48940, Spain

J. Ospino‡

Departamento de Matematica Aplicada, Universidad de Salamanca, Salamanca 37007, Spain

(Received 24 June 2013; published 19 September 2013)

We analyze the behavior of the geodesic motion of test particles in the spacetime of a specific class of axially symmetric static vacuum solutions to the Einstein equations, hereafter referred to as the linearized multipole solution. We discuss its suitability to describe a quasispherical spacetime. The existence of an innermost stable circular orbit very close to the (singular) horizon of the source is established. The existence of such a stable orbit, closer than that of the Schwarzschild metric, as well as the appearance of a splitting in the admissible region of circular orbits, is shown to be due to the multipole structure of the solution, thereby providing additional potential observational evidence for distinguishing Schwarzschild black holes from naked singularities.

DOI: 10.1103/PhysRevD.88.064041 PACS numbers: 04.20.Cv, 04.20.Dw, 04.80.Cc, 97.60.Lf

I. INTRODUCTION

As it follows from the Israel theorem [1], the only static and asymptotically flat vacuum spacetime possessing a regular horizon is the Schwarzschild solution. For all the other Weyl exterior solutions [2–6], the physical components of the Riemann tensor exhibit singularities at the infinite-redshift surface. Even though we shall restrict ourselves to the static case, it is worth noting that a result similar to the Israel theorem exists for stationary solutions with respect to the Kerr metric [7–9].

Now, sphericity is a common assumption in the description of compact objects, where deviations from spherical symmetry are likely to be incidental rather than basic features of these systems.

Furthermore, if the field produced by a self-gravitating system is not particularly intense (the boundary of the source is much larger than the infinite-redshift surface) and fluctuations from spherical symmetry are slight, then there is no problem in representing the corresponding deviations from spherical symmetry (both inside and outside the source) as a suitable perturbation of the spherically symmetric exact solution [10].

However, as the object becomes more and more compact, such a perturbative scheme will eventually fail close to the source. Indeed, as is well known [11–16], though usually overlooked, as the boundary surface of the source approaches the infinite-redshift surface, any finite perturbation of the Schwarzschild spacetime becomes fundamentally different from the corresponding exact solution representing the quasispherical spacetime, even if the latter is characterized by parameters whose values are arbitrarily close to those corresponding to the Schwarzschild metric. This, in turn, is just an expression of the Israel theorem.

In other words, for strong gravitational fields, there exists a bifurcation between the perturbed Schwarzschild metric and all the other Weyl metrics (in the case of gravitational perturbations), no matter how small are the multipole moments (higher than monopole) of the source. Examples of such a bifurcation have been brought out in the study of the trajectories of test particles in the γ spacetime [17–24], and in the M-Q spacetime [25,26], for orbits close to the infinite-redshift surface [27,28].

Due to the bifurcation mentioned above, a fundamental question arises: How should we describe the quasispherical spacetime resulting from the fluctuations from Schwarzschild?

(a) By means of a perturbed Schwarzschild metric producing a black hole?
or
(b) By means of an exact solution to the Einstein equations, whose (radiatable) multipole moments are arbitrarily small, though nonvanishing, and leading to a naked singularity?

As we shall see here, the quandary above might be solved by comparing the behavior of circular geodesics in either case.

*jlhp@usal.es
†lherrera@usal.es
Also at U.C.V., Caracas.
‡j.ospino@usal.es

Indeed, in spite of some results obtained in the study of the source of quasispherical spacetimes [29,30], which favor scenario (b), we are well aware of the fact that presently most researchers favor scenario (a). Nevertheless, the doubt remains, and the very different behavior of the system implied by the bifurcation mentioned above opens the way for proposing observational scenarios that will allow for distinguishing between black holes and naked singularities. In fact, this issue has attracted the attention of many researchers in recent years (see Refs. [31–44] and references therein).

However, an important open question arises, related to the proposed approach, namely: Since there are as many different (physically distinguishable) Weyl solutions as there are different harmonic functions, which among the Weyl solutions is best entitled to describe small deviations from spherical symmetry?

In the past, different authors have resorted to different metrics to describe deviations from spherical symmetry, e.g., the γ metric or the M-Q spacetime in Refs. [27–30,43], the Young-Coulter solution [45] in Ref. [46], the Quevedo-Mashhoon solution [47] in Ref. [48], or the Manko-Novikov solution [49] in Ref. [44].

The rationale behind the choice of the γ metric is based on the fact that it corresponds to a solution of the Laplace equation (in cylindrical coordinates) with a singularity structure similar to that of the Schwarzschild solution (a line segment). In this sense the γ metric appears as a ''natural'' generalization of Schwarzschild spacetime to the axisymmetric case.

On the other hand, due to its relativistic multipole structure, the M-Q solution (more exactly, a subclass of this solution, M-Q$^{(1)}$ [25]) may be interpreted as a quadrupole correction to the Schwarzschild spacetime, and therefore represents a good candidate among known Weyl solutions to describe small deviations from spherical symmetry.

However, it should be obvious that the question above does not have a unique answer (there are an infinite number of ways of being nonspherical, so to speak) and therefore in the study of any specific problem, the choice of the corresponding Weyl spacetime has to be reasoned.

In this work, we intend to use yet another exact solution of the Weyl family in order to describe deviations from spherical symmetry. Such a solution is the so-called linearized multipole (LM) metric [50]; its properties and the reasons behind its choice to describe a quasispherical spacetime are presented in the next section. Next, we shall calculate the circular geodesics in that spacetime and compare its behavior with the spherically symmetric case. The most relevant result emerging from that analysis is the existence of stable innermost circular orbits very close to the (singular) horizon of the source, and closer than that of the Schwarzschild metric.

II. THE LINEARIZED MULTIPOLE SPACETIME

As mentioned in the Introduction, we shall carry out a study of circular geodesics in the LM spacetime. Thus, we shall first very briefly revise such a metric and provide arguments justifying its use to describe quasispherical (axially symmetric and static) spacetime (see Ref. [50] for details). Finally, we shall present the multipole structure of the solution.

A. The metric

As is known, the line element of a static and axisymmetric vacuum spacetime is represented in Weyl form as follows:

$$ds^2 = -e^{2\Psi}dt^2 + e^{-2\Psi}[e^{2\gamma}(d\rho^2 + dz^2) + \rho^2 d\varphi^2], \quad (1)$$

where Ψ and γ are functions of the cylindrical coordinates ρ and z alone. The metric function Ψ is a solution of the Laplace equation ($\triangle\,\Psi = 0$), and the other metric function γ satisfies a system of differential equations whose integrability condition is just the equation for the function Ψ. Thus, the Weyl family of solutions with good asymptotical behavior is given in associated spherical Weyl coordinates $\{r, \theta\}$ as

$$\Psi = \sum_{n=0}^{\infty} \frac{a_n}{r^{n+1}} P_n(\omega), \quad (2)$$

where $r \equiv \sqrt{\rho^2 + z^2}$, $\omega \equiv \cos\theta = z/r$, and P_n denotes the Legendre polynomial.

Thus, the line element now reads

$$ds^2 = -e^{2\Psi}dt^2 + e^{-2\Psi+2\gamma}(dr^2 + r^2 d\theta^2) + e^{-2\Psi} r^2 \sin^2\theta d\varphi^2. \quad (3)$$

Also, as is well known, in spite of the form of Eq. (2), the coefficients a_n are not the relativistic multipole moments (RMMs) of the solution as defined for static and axisymmetric vacuum solutions by Geroch [51,52] and Thorne [53]. However, the ''Newtonian'' moments a_n, which provide the so-called ''Newtonian image'' of the solution, can be expressed as functions of the RMMs [54–57]. Although the full relations linking both sets of coefficients are extremely complicated, they can be used to obtain relatively simple formulas for the coefficients $\{a_n\}$ in situations where the deviation of the relativistic solution from spherical symmetry is small. This issue has been discussed in some detail in Refs. [25,58,59].

A solution of the Weyl family that represents the exterior gravitational field of a mass distribution whose multipole structure only possesses mass M and quadrupole moment Q was found in Ref. [25]. This solution (M-Q) has become a useful tool for describing small deviations from the spherically symmetric solution [28,60–62].

The basic idea underlying the obtention of the M-Q solution is that Q is small, since we want to describe slight

deviations from the Schwarzschild solution, and all the RMMs of higher order are negligible. This assumption about the RMMs higher than Q is supported by the following argument: The Newtonian calculation of the multipole moments of an ellipsoidal mass distribution shows that as we move from lower to higher moments, their magnitudes decrease as powers of the eccentricity of the ellipsoidal configuration (see Refs. [58,63] for details). Then the M-Q solution is constructed as a sum of functions in a power series of the dimensionless quadrupole parameter $q \equiv Q/M^3$, starting at the Schwarzschild solution as the first order, in such a way that the successive powers of q control the desired corrections to the spherical symmetry.

The LM solution [50] was constructed with the same purpose, namely to describe the gravitational field of a body slightly different from a sphere. However, the approach to find it, although similar, is different from the one used for the M-Q solution. In both cases, it should be clear that, in describing nonspherical spacetimes, their physical components of the Riemann tensor exhibit singularities at the infinite-redshift surface.

The rationale behind the LM solution is the following: When attempting to describe an isolated compact body which is not spherically symmetric, all the RMMs appear, no matter how small is the deviation from spherical symmetry. Therefore, let us consider that all RMMs appear in the solution that we want to construct, but let us restrict their magnitudes to be very small, so that we can neglect all terms in the Weyl coefficients whenever a cross product of RMMs is involved. This is the origin of the name of the family of solutions: *linearized multipole* (LM) solutions. It should be observed that due to the linearity of the Laplace equation, the so-obtained solution is an exact solution to the Einstein equations.

Now, the expression for the metric function of the Weyl family solution endowed with $g+1$ independent RMMs (the LM solution) can be written, in prolate spheroidal coordinates [64], as follows:

$$\Psi = -\frac{Hx}{x^2-y^2} - \sum_{n=0}^{g} Q_{2n}(x)P_{2n}(y)\left[\sum_{j=n}^{g} H_j C_{2j,2n}\right], \tag{4}$$

where $C_{n,k}$ are the coefficients appearing at the series expansion of any variable as a linear combination of Legendre polynomials in that variable, i.e., $\xi^n = \sum_{k=0}^{\infty} C_{n,k}P_k(\xi)$) and

$$H \equiv \sum_{k=0}^{g} m_{2k}h(k), \qquad H_j \equiv \sum_{k=j}^{g} m_{2k}h_j(k), \tag{5}$$

where the parameter $m_{2k} \equiv \frac{M_{2k}}{M^{2k+1}}$ denotes the dimensionless relativistic multipole moment of order 2^{2k}-pole (M_{2k}), whereas the explicit expressions for the coefficients $h_j(k)$ ($\forall\ k \geq j$, since $h_j(k) = 0$ for $k < j$) and $h(k)$, are

$$h_j(k) = \frac{1}{2^{4k-1}}(-1)^{k-j-2}\binom{4k+1}{2k}\frac{k^2+k/2-j}{(k+1)} \times \frac{(2k+2j)!}{(2j)!(k+j)!(k-j)!},$$
$$h(k) = \frac{1}{2^{2k}(k+1)}\binom{4k+1}{2k}, \quad \forall\ k>0. \tag{6}$$

The parameter H can be calculated in terms of the coefficients H_j as follows:

$$H = \sum_{k=0}^{g}\frac{m_{2k}}{2^{2k}(k+1)}\binom{4k+1}{2k} = \left[1 - \sum_{j=0}^{g}\frac{H_j}{2j+1}\right]. \tag{7}$$

In terms of its "Newtonian image," the LM solution can be described by means of an "object image" whose Newtonian gravitational potential (the gravitational potential corresponding to the Newtonian image, not to confound with the weak-field limit of the solution) and Newtonian multipole moments equal the metric function of the solution and the Weyl coefficients, respectively. That "object image" is represented by a kind of "dumbbell" consisting of a bar of length $2M$ with linear density μ given by an even polynomial of degree $2g$ and two balls at each end of the bar with mass ν (see Ref. [50] for details).

The other metric function γ of the line element [Eq. (1)] can be obtained from the metric function Ψ by solving the corresponding field equations

$$\gamma_\rho = \rho(\Psi_\rho^2 - \Psi_z^2), \qquad \gamma_z = 2\rho\Psi_\rho\Psi_z. \tag{8}$$

There already exists an expression for this metric function [64] in terms of the Weyl coefficients of the series Ψ [Eq. (2)], but it is highly complicated to handle, and a summation of a series is required to obtain the analytic expression of the metric function. One advantage inherent to the dumbbell description of the solution consists of an integral expression [65] for the metric function γ in terms of the density of the dumbbell:

$$\gamma = \int_{-1}^{1} dX \int_{-1}^{1} dY \frac{\mu^d(X)\mu^d(Y)}{(Y-X)^2} \times \left[\frac{r^2(1-\omega^2) + (r\omega - XM)(r\omega - YM)}{R(X)R(Y)} - 1\right], \tag{9}$$

or equivalently,

$$\gamma = -M^2r^2(1-\omega^2)[\nu^2 A(r,\omega) + 2\nu(I_- + I_+) + II], \tag{10}$$

where the following notation is used: $R(X) \equiv \sqrt{r^2 + X^2M^2 - 2r\omega XM}$, where $\mu^d(X)$ represents the density of the dumbbell, and

$$
\begin{aligned}
II &\equiv \iint_{-1}^{1} \frac{\mu(X)\mu(Y)dXdY}{R(X)R(Y)[r^2(1-\omega^2)+(r\omega-XM)(r\omega-YM)+R(X)R(Y)]},\\
I_{\pm} &\equiv \int_{-1}^{1} dX \frac{\mu(X)}{r_{\pm}R(X)[r^2(1-\omega^2)+(r\omega-XM)(r\omega\pm M)+r_{\pm}R(X)]},\\
A(r,\omega) &\equiv \frac{1}{4r_{-}^4}+\frac{1}{4r_{+}^4}+\frac{1}{r_{-}r_{+}[r^2-M^2+r_{+}r_{-}]}.
\end{aligned}
\tag{11}
$$

The fact that the Newtonian image of the LM solution is a dumbbell is quite convenient, since many properties of the solution can be described in terms of the density of the bar. Thus, for example, it can be shown that the source of the solution will be prolate (oblate) if μ is smaller (greater) than $1/2$. Also, as we shall see below, the possible existence of an innermost stable circular orbit (ISCO), within the one corresponding to the spherically symmetric case, is related to a condition on μ at the origin [Eq. (32)].

B. Mutipole structure of the solution

As already mentioned, the RMMs of a Weyl solution can be calculated in terms of the coefficients a_n. This relation can be inverted to obtain the Newtonian moments (a_n) in terms of the RMMs. The assumption used to construct the LM solution is that every RMM is small, implying that we may neglect all the terms with coupling interaction between RMMs appearing in the Weyl coefficients a_n. (Once again it should be emphasized that, due to the linearity of the Laplace equation, the so-obtained metric is an exact solution to the Einstein equations.) With this selection of the coefficients, we can consider that the solution possesses a finite number of parameters ($q \equiv m_2, m_{2i}$, with $1<i\leq g$) that represent each RMM of the solution.

Thus, the first RMMs of the solution are the following (odd moments are null because of the equatorial symmetry):

$$
\begin{aligned}
&M_0 = M, \qquad M_2 = M^3 q,\\
&M_4 = M^5 m_4, \qquad M_6 = M^7\left(m_6 - \frac{60}{77}q^2\right),\\
&M_8 = M^9\left(m_8 - \frac{226}{143}qm_4 - \frac{1060}{3003}q^2 - \frac{40}{143}q^3\right),\\
&M_{10} = M^{11}\left(m_{10} - \frac{28616}{46189}qm_4 - \frac{566}{323}qm_6 - \frac{30870}{46189}m_4^2\right.\\
&\qquad \left. - \frac{19880}{138567}q^2 - \frac{39150}{46189}q^2m_4 + \frac{146500}{323323}q^3\right).
\end{aligned}
\tag{12}
$$

III. GEODESICS

We shall now study the geodesic motion of test particles in the spacetime of the LM solution. We shall restrict ourselves to the case of geodesics with constant θ and $\frac{d\varphi}{d\sigma} \neq 0$; i.e., those constrained to a constant hypersurface ($\theta = \theta_0$) with coordinates $\{t, r, \varphi\}$.

Therefore, we obtain on the equatorial plane the following expression (see Ref. [61]):

$$
\left(\frac{dr}{d\sigma}\right)^2 + V_{\text{eff}} = C, \tag{13}
$$

where σ denotes the affine parameter along the geodesic, C is a constant, and V_{eff} is an effective potential which can be obtained by integration as follows:

$$
V_{\text{eff}} = \int \frac{k}{g_{11}}\partial_r \ln\left(\frac{g_{11}}{k}\right)dr = -\frac{k}{g_{11}}, \tag{14}
$$

with $k \equiv \epsilon - \frac{h^2}{g_{00}} - \frac{l^2}{g_{33}}$, where h and l represent the energy and angular momentum per unit mass, respectively, and ϵ denotes the norm of the tangent vector to the geodesic z^{α}.

From Eqs. (13) and (14), we have that

$$
\left(\frac{du}{d\varphi}\right)^2 = \frac{k}{g_{11}}\frac{g_{33}^2}{l^2}u^4, \tag{15}
$$

where $u \equiv 1/r$.

The above equations lead, for the line element in Eq. (1), to

$$
\left(\frac{du}{d\varphi}\right)^2 = \frac{F(r)}{l^2 e^{2\gamma+4\Psi}}, \tag{16}
$$

$$
V_{\text{eff}} = -\frac{F(r)}{e^{2\gamma}}, \tag{17}
$$

where the function $F(r) \equiv ke^{2\Psi}$ for timelike geodesics on the equatorial plane is

$$
F(r) = -e^{2\Psi} + h^2 - \frac{l^2}{r^2}e^{4\Psi}. \tag{18}
$$

When looking for circular orbits, we search for the stationary solutions of the autonomous partial differential equation (16); i.e., $\frac{du}{dr} = 0 \Leftrightarrow u = cte$. Hence, we can say that the circular orbits are defined by radial values $r = R_i$ where the following condition is satisfied:

$$
F(R_i) = \frac{dF}{dr}(R_i) = 0, \tag{19}
$$

since the extremals of the effective potential satisfy

$$
\begin{aligned}
&\frac{dV_{\text{eff}}}{dr}(R_i) = 0 = (-F'(R_i) + F(R_i)2\gamma'(R_i))e^{-2\gamma(R_i)}\\
&\quad \Rightarrow F' \equiv \frac{dF}{dr}(R_i) = 0,
\end{aligned}
\tag{20}
$$

where the prime denotes a derivative with respect to r. Therefore, the circular orbits can be calculated by means of the function $F(r)$ without using the second metric function γ, since the complete effective potential is not needed.

The timelike geodesic described by a pointlike particle around a circular orbit is defined by the zeros of both the function $F(r)$ and its derivative. The orbit $r = R_i$ is stable ($\frac{d^2V_{\rm eff}}{dr^2} > 0$) if $-F''(R_i) > 0$ (the minimum), and it is unstable ($\frac{d^2V_{\rm eff}}{dr^2} < 0$) if $-F''(R_i) < 0$ (the maximum). In the above, it has been used that

$$\frac{d^2V_{\rm eff}}{dr^2} = e^{-2\gamma}(-F'' + F'4\gamma' + F2\gamma'' - (2\gamma')^2F), \tag{21}$$

and hence

$$\frac{d^2V_{\rm eff}}{dr^2}(R_i) = -e^{-2\gamma(R_i)}F''(R_i). \tag{22}$$

Observe that the specific energy of the geodesic orbit is $E = -z_0$; therefore, since $z_0 = h = \frac{dt}{d\sigma}g_{00} < 0$, the parameter h [with $V_{\rm eff} = 0$ or equivalently $F(R_i) = 0$] denotes, up to a sign, the energy per unit of mass of the test particle, and it is fixed once the extremals (R_i) of $F(r)$ are determined:

$$h^2 = e^{2\Psi(R_i)}\left[1 + \frac{l^2}{R_i^2}e^{2\Psi(R_i)}\right]. \tag{23}$$

Also, observe that the conditions for circular orbits [Eqs. (19) and (20)] determine the values of h and l as follows:

$$l_i^2 = \left.\frac{r^3\Psi'}{e^{2\Psi}(1-2r\Psi')}\right|_{r=R_i},$$
$$h_i^2 = \left.e^{2\Psi}\frac{1-r\Psi'}{1-2r\Psi'}\right|_{r=R_i}. \tag{24}$$

Then, these parameters are constants of motion for each value of the radial coordinate $r = R_i$. In what follows, we shall consider the angular parameter as a function of the radial coordinate r for different circular orbits, and hence we introduce the notation

$$L = L(r) \equiv \frac{l^2}{4M^2} = \frac{r^3\Psi'}{4M^2e^{2\Psi}(1-2r\Psi')}. \tag{25}$$

A. The spherically symmetric solution

For the forthcoming discussion, it would be convenient to recover the Schwarzschild case, which is well known.

Depending on the value of L, the function $-F(r)$ acquires a maximum and a minimum starting from the particular value $L = 3$, for which both extremals coincide at $r_s = 6M$. For large values of L, the minimum goes away asymptotically along $r_s/M = 3$. In what follows, the notation $\lambda \equiv r_s/M$ shall be used, where r_s denotes the radial Schwarzschild coordinate and it is related to the radial Weyl coordinate r (on the equatorial plane) as follows:

$$s \equiv \frac{r}{M} = \frac{r_s}{M}\sqrt{1-2\frac{M}{r_s}}. \tag{26}$$

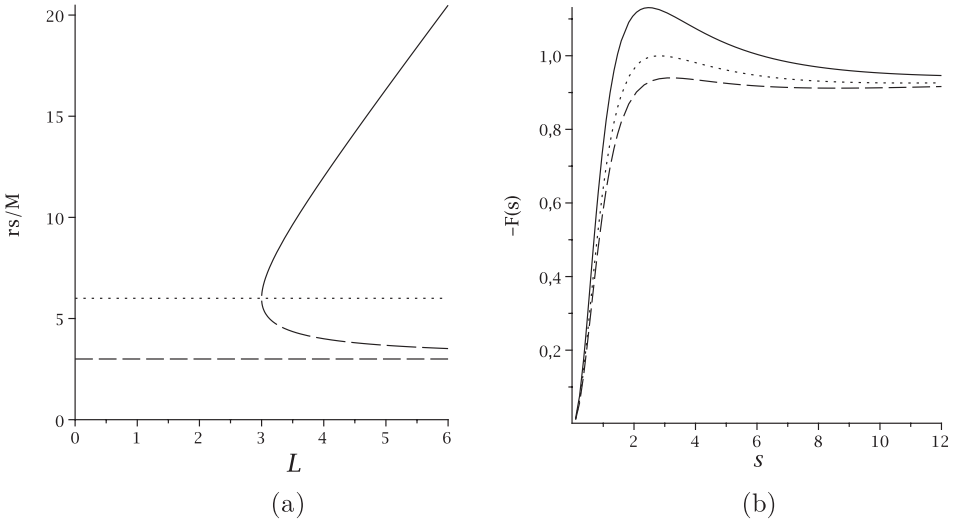

FIG. 1. (a) The plot of the parameter L in terms of the dimensionless Schwarzschild radial coordinate r_s/M. For each value of the parameter L (horizontal axis), the solid line and the long-dashed line provide the points where the function $-F(s)$ acquires the minimum or the maximum, respectively. These values define the corresponding radii of the circular stable or unstable orbits, respectively. As is known, no matter how large the parameter L would be, the inner unstable orbit is located at $r_s = 3M$ (dashed horizontal line), and the bifurcation point between stable and unstable orbits (the marginally stable orbit) is located at $r_s = 6M$, where the inner stable orbit is reached (shown with a dot line in the graphic). (b) In this graphic, the function $-F(s)$ is represented for different values of L. Starting from the solid line and downward, the values of the parameter L are $L = 5, 4, 3.5$. Let us note that the value $L = 3$ corresponds to the marginally stable orbit, where $F(s)$ has no extremals points but an inflection point.

In Fig. 1(a), we plot the parameter L as a function of the dimensionless Schwarzschild radial coordinate r_s/M, where the fact that, for the circular orbits of the Schwarzschild spacetime, $r_s/M = 2L(1 \pm \sqrt{1-3/L})$ has been used. The value of the parameter h is taken to be zero, since it only generates a displacement of the graphic along the vertical axis. There exist certain values h for each extremal R_i, where $F(R_i) = 0$. In Fig. 1(b), $-F(r)$ with its extremals are shown for different values of L.

B. The LM solution

Let us now analyze the situation in the LM solution. To derive the consequences implied by the extremal condition $F'(r) = 0$, we need to solve numerically the following transcendent equation:

$$e^{2\Psi} = \frac{r^3}{l^2}\frac{\Psi'}{1-2r\Psi'}. \tag{27}$$

Nevertheless, relevant information can be extracted from the analytical study of the function $-F(r)$ [Eq. (18)]. The calculation of that function for the LM solution yields

$$-F(s) = G^{C(s)}e^{A(s)} + \frac{4L}{(\sqrt{s^2+1}+1)^2}G^{2C(s)-1}e^{2A(s)} - h^2 \tag{28}$$

with the notation (for the case $g = 2$)

$$A(s) \equiv -\sqrt{s^2+1}B(s) - \frac{2H}{\sqrt{s^2+1}}, \tag{29}$$

$$G \equiv \frac{\sqrt{s^2+1}-1}{\sqrt{s^2+1}+1}, \qquad C(s) \equiv H_0 - \frac{1}{2}H_1 s^2 + \frac{3}{8}H_2 s^4, \tag{30}$$

$$B(s) \equiv H_1 + H_2\left(\frac{1}{2} - \frac{3}{4}s^2\right). \tag{31}$$

These expressions are easily obtained from the metric function Ψ [Eq. (4)] by considering it on the equatorial plane ($y = 0$) and taking into account that $x = \lambda - 1 = \sqrt{1+s^2}$ (the explicit expression of Ψ in Weyl coordinates can be seen in Ref. [50]). Let us note that $e^{2\Psi} = G^{C(s)}e^{A(s)}$, and $G^{2C(s)} = \frac{G^{2C(s)-1}s^2}{(\sqrt{s^2+1}-1)^2}$.

As can be seen in Fig. 2, the behavior of the function $-F(r)$ is different from that corresponding to the spherically symmetric case.

Indeed, as shown in that figure, for certain values of the multipole parameters $q \equiv m_2$ and m_4, the curve clearly shows a minimum close to the origin. This implies the existence of an ISCO, closer than the one corresponding to the spherically symmetric case, and therefore related to the presence of the multipole moments (m_2 and m_4). Let us remember that $r = 0$ corresponds to the infinite-redshift surface [Eq. (26)].

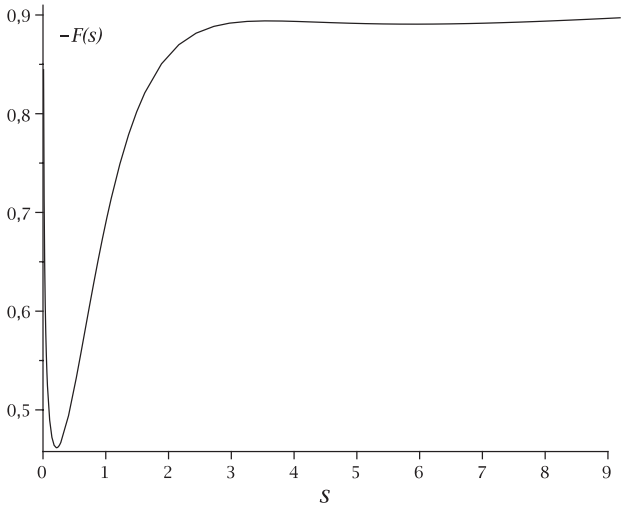

FIG. 2. The function $-F(s)$ is represented for the LM solution possessing monopole, quadrupole, and 2^4-pole moments ($h = 0$ is considered).

If we calculate the behavior of the function $-F(s)$ when approaching the horizon, we see that this function goes to infinity for certain values of the multipole parameters, thereby exhibiting the existence of a minimum which is absent in the Schwarzschild solution:

$$\lim_{s\to 0}(-F(s)) = \begin{cases} 0, & 2H_0 - 1 > 0 \\ \infty, & 2H_0 - 1 < 0 \end{cases}, \tag{32}$$

since $\lim_{s\to 0}e^{2\Psi} = \lim_{s\to 0}G^{C(s)}e^{A} = 0$ because $C(0) = H_0 \equiv 2\mu^{\mathrm{LM}}(0) > 0$ (the density of the dumbbell bar is positive definite).

For the case of the M-Q$^{(1)}$ solution, i.e., the LM solution with monopole and quadrupole moments alone, the existence of the ISCO is determined by the following range of values of the quadrupole parameter: $q \in [\frac{4}{15}, \frac{8}{15}]$.

For the case of the LM solution with monopole, quadrupole, and 2^4-pole moments, the existence of the ISCO is determined by the following ranges of values of the quadrupole parameter:

$$q \in \begin{cases} \left[-\frac{32}{255}, -\frac{16}{255}\right], & m_4 = q \\ \left[\frac{16}{375}, \frac{32}{375}\right], & m_4 = -q \end{cases},$$

where we have assumed that the absolute values of both multipole moments are identical (see Ref. [50] for details). The determination of these ranges of values is obtained from imposing two conditions: the positive-definite density condition and $2H_0 - 1 < 0$, which leads to $0 < H_0 < 1/2$. (See Fig. 3 for details and a graphical characterization of these ranges.)

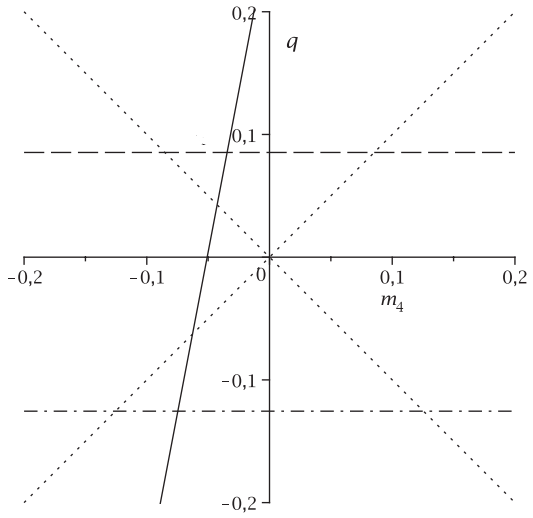

FIG. 3. The domain of the existence of an ISCO in the LM solution is shown. Dotted lines draw the condition assumed on the parameters q and m_4, which are supposed to be of equal magnitude (in absolute value). The continuous line represents the limit [Eq. (32)] $1 - \frac{15}{4}q + \frac{315}{16}m_4 < 0$ for the existence of an ISCO; hence, the values of q must be situated on top of this line. The intersections of these lines determine the upper value of q if it is negative or the lower bound if it is positive, whereas the other extremes of the ranges are determined by the definite-positive condition of the density (horizontal dashed line and dot-dashed line).

In addition, a more relevant feature of these solutions is obtained from the study of the marginally stable orbit (MSO). Indeed, as is known, for a circular MSO, the angular parameter (as well as the energy) have extremal values. This condition is just equal to $F'' = 0$, as can be seen by taking the derivative of Eq. (25):

$$\frac{dL}{dr} = 0 \Leftrightarrow 0 = r\Psi'' + 3\Psi' + 4r^2(\Psi')^3 - 6r(\Psi')^2. \quad (33)$$

Therefore, the circular equatorial motion is known to be stable when $L' > 0$ and unstable for $L' < 0$. Let us notice that the epicyclic frequency is proportional to L', and hence the MSO ($L' = 0$) determines the orbit with non-horizontal oscillations. The existence of an ISCO, as we have previously shown, can be confirmed when studying the behavior of L in terms of the orbital radius.

Such behavior is displayed in Fig. 4, using Eq. (25) for different values of the quadrupolar parameter q, for the case of the M-Q$^{(1)}$ solution. For the discussion below, an important role will be played by the function $g(r) \equiv 1 - 2r\Psi'$, which is related to L by

$$\frac{dL}{dr} = \frac{1}{4M}\frac{r^3\Psi'' + 3r^2\Psi' + 4r^4(\Psi')^3 - 6r^3(\Psi')^2}{e^{2\Psi}g(r)^2}. \quad (34)$$

The plot of g as a function of λ is given in Fig. 5 for the M-Q$^{(1)}$ and the LM solutions.

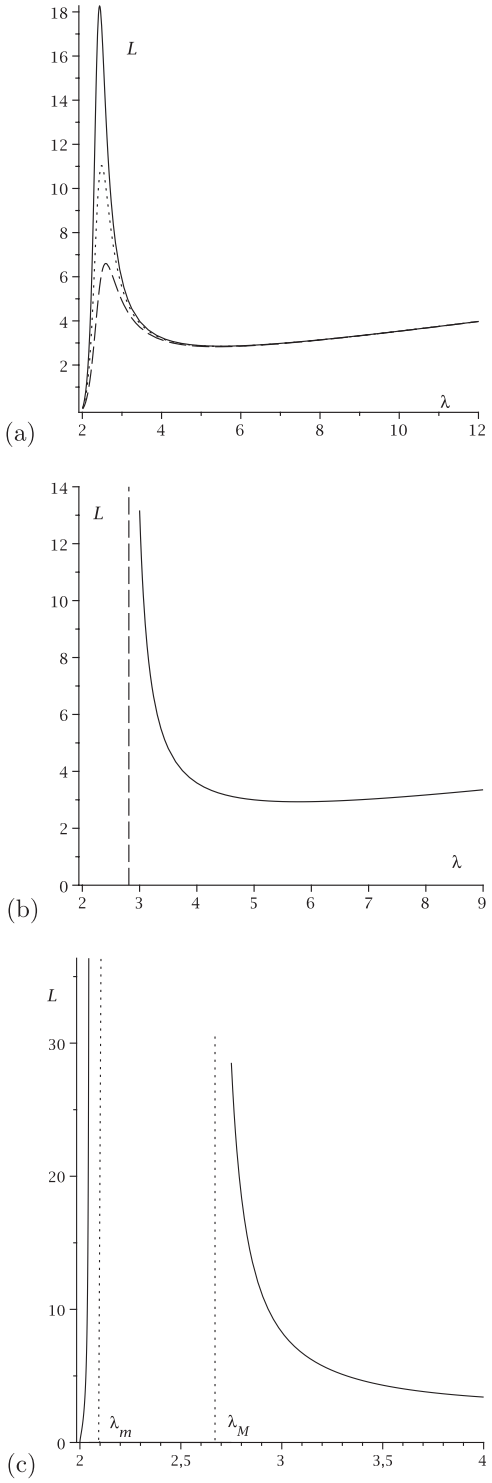

FIG. 4. Localization of circular orbital radii in terms of the parameter L (in the vertical axis) for different values of the quadrupolar parameter for the M-Q$^{(1)}$ solution. (a) For $q \in (q_c, 8/15]$: Starting from the solid line and downwards, the values of the corresponding quadrupolar parameter are $q = 0.4$, 0.42, 0.46. (b) For $q \in (0, 4/15]$: This curve corresponds to $q = 0.2$, where the asymptote is located at $\lambda = 2.8125$ (a smaller value than the corresponding one for the Schwarzshild case, $\lambda = 3$). (c) For $q \in (4/15, q_c]$: This piecewise curve corresponds to $q = 0.3$, where the asymptotic lines bounding the forbidden region are located at $\lambda_m = 2.0473$ and $\lambda_M = 2.6646$.

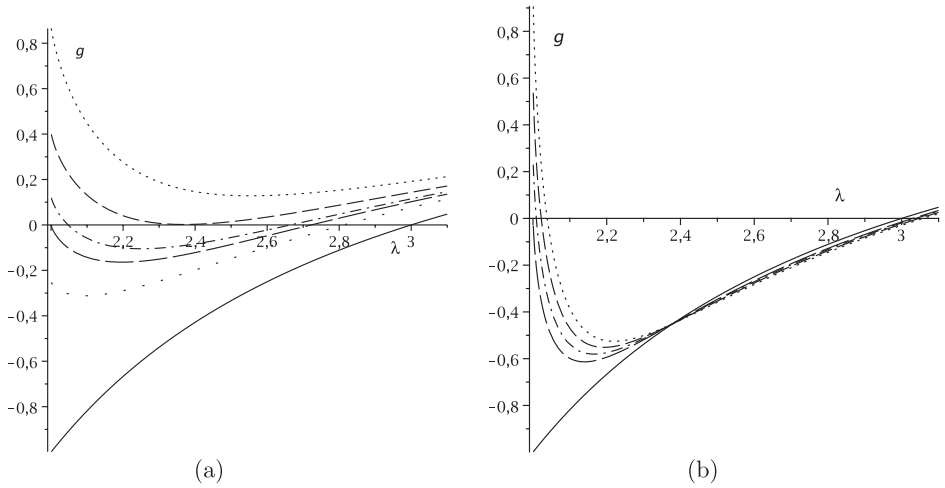

FIG. 5. Plot of g as a function of λ for the (a) M-Q$^{(1)}$ and (b) LM solutions for different values of the multipole parameters. The solid line in both plots corresponds to the Schwarzschild case $q = 0$, whereas the other values of q are (a) $q = 0.5$ (upper dotted line), $q = 0.374 \sim q_c$ (dashed line), and from that line and downwards $q = 0.3, 4/15, 0.2$. The special value $q = 4/15$ corresponds to the lower bound for the existence of ISCOs near the horizon. (b) from the solid line $q = m_4 = 0$ and upwards, $q = m_4 = -0.063, -0.08, -0.1, -0.124$.

The following conclusions emerge from Figs. 4 and 5:

(1) First, we see that stable orbits are located to the left of the maximum, and the right of the minimum [Fig. 4(a)] where $L' > 0$. The slope of the curve where $L' < 0$ determines the range of the orbital radius for unstable orbits. The MSO is located at the maximum or minimum of the curve (L_+ and L_-, respectively). The values of the orbital radius (mso$_+$ and mso$_-$ for the maximum and minimum, respectively) at these two extremals of L correspond to the inflection points of the potential $-F$, for which this function does not possess extremal points. For other values of $L \in (L_+, L_-)$ (at each value of q), the potential $-F$ will possess one maximum and two minima corresponding to the intersection points of the curves in Fig. 4(a) with the horizontal lines $L = cte$.

(2) Second, Fig. 4(b) represents the curve for a value of the quadrupolar parameter q where the inner unstable orbit is limited by the asymptotic dashed line, and the inner stable orbit is located at the minimum of the curve. This plot recovers the behavior of the spherical case but slightly modifies the position of the circular orbits when a quadrupole moment is present. The relevant difference with respect to the spherical case is that a maximum of L (L_+) arises at the value of the radial coordinate mso$_-$ whenever some multipole of the solution, higher than the monopole, is not zero (within a determined range of that multipole parameter), and this fact leads to the existence of stable circular orbits at a radius smaller than those where the other known minima and the maximum appear. In addition, these new stable circular orbits possess smaller values of L and energy h than the former ones.

(3) Finally, we notice the existence of a splitting [see Fig. 4(c)] in the admissible region of circular orbit radii for some values of the multipole moments of our spacetime. This fact was already discussed in Ref. [44], where by means of numerical methods the authors obtain results that suggest the existence of disconnected nonplunging regions at small radii. The existence of such regions could be tested, for instance, in the presence of accretion disks forming a ring structure around the source. The analytical determination of that region consists of calculating the zeros of the function $g(r)$.

Thus, for some values of q the maximum of L disappears and a region of forbidden circular orbits arises, as is shown in Fig. 4(c). This region corresponds to the range of values of the radial coordinate leading to $g(r) < 0$ (let us remember that $L \geq 0$, $h^2 \geq 0$). The zeros of the function $g(r)$ (see Fig. 5) provide the asymptotical behavior of L at the values λ_m and λ_M [Fig. 4(c)].

To complement the discussion above, it is instructive to take a look at Tables I and II, which display the values of different parameters characterizing ISCOs for the LM solution with $g = 1$ [M-Q$^{(1)}$]. As mentioned before, if $q \in (0, \frac{4}{15}]$, the behavior of circular orbits is similar to the spherically symmetric case: the minimum of L [Fig. 4(b)] defines the change from stable to unstable orbits, and thereby the minimal value of the radius of the stable circular orbit (mso$_-$).

The maximum of the orbital radius for the unstable orbit exhibits (as in the Schwarzschild case) an asymptote in the value of λ which is smaller than that corresponding to the spherically symmetric case ($\lambda = 3$).

There exists a critical value for q (q_c) beyond which a gap in the range of possible values of the radius of the circular orbit appears for which there are not ISCOs.

TABLE I. Numerical values of characteristic parameters corresponding to ISCOs in the M-Q$^{(1)}$ solution.

q	L	h^2	ISCO(r_s/M)
0	3	0.889	6
0.28	0.1	0.016	2.000
0.28	1.1	0.147	2.001
0.28	2.1	0.269	2.004
0.28	3.1	0.388	2.006
0.28	4.1	0.508	2.007
0.28	5.1	0.626	2.008
0.34	0.1	0.053	2.003
0.34	1.1	0.259	2.041
0.34	2.1	0.433	2.062
0.34	3.1	0.602	2.076
0.34	4.1	0.769	2.086
0.34	5.1	0.935	2.093
0.40	0.1	0.093	2.015
0.40	1.1	0.335	2.104
0.40	2.1	0.535	2.148
0.40	3.1	0.728	2.179
0.40	4.1	0.918	2.202
0.40	5.1	1.106	2.222
0.46	0.1	0.130	2.038
0.46	1.1	0.392	2.174
0.46	2.1	0.606	2.245
0.46	3.1	0.811	2.301
0.46	4.1	1.010	2.352
0.46	5.1	1.202	2.407
0.52	0.1	0.163	2.068
0.52	1.1	0.436	2.248
0.52	2.1	0.657	2.350
0.52	3.1	0.865	2.446
0.52	4.1	1.064	2.577

This is clearly indicated in Fig. 4(c), where the gap is determined by the interval (λ_m, λ_M) for $q \in (\frac{4}{15}, q_c]$.

In the interval $(0, \lambda_m)$, there are ISCOs close to the infinite-redshift surface.

For the M-Q$^{(1)}$ solution, q_c is given by

$$q_c = 0.373434, \qquad r_s/M = 2.367, \tag{35}$$

which corresponds to the value of q for which $g(r)$ has a single zero (see Fig. 5).

If $q \in (q_c, \frac{8}{15}]$, there are ISCOs in the interval $(0, L_+)$, with values of the orbital radius smaller than those corresponding to stable circular orbits for L_- where L has a minimum (mso$_-$).

Three comments are in order at this point:

(1) It should be stressed that the range of admissible values of the angular momentum $(0, L_+)$ is quite large. Therefore, ISCOs correspond to test particles with a wide range of angular velocities.

TABLE II. Extremal values of the marginally stable orbits mso$_+$ and mso$_-$ with the corresponding value of the angular momentum parameter L for which ISCOs exist, and the range of nonexistence of stable orbits for different values of the quadrupole moment, for the M-Q$^{(1)}$ solution.

q	mso$_+$	L_+	mso$_-$	L_-	(λ_m, λ_M)	λ
0	...	...	6	3	...	3
0.04	...	...	5.957	2.987	...	2.968
0.08	...	...	5.913	2.973	...	2.934
0.12	...	...	5.868	2.960	...	2.898
0.16	...	...	5.821	2.946	...	2.857
0.20	...	...	5.772	2.931	...	2.812
0.24	...	...	5.722	2.917	...	2.761
0.26	...	...	5.696	2.909	...	2.732
0.28	...	...	5.670	2.902	2.014, 2.701	...
0.30	...	...	5.643	2.894	2.047, 2.665	...
0.32	...	...	5.615	2.886	2.092, 2.623	...
0.34	...	...	5.587	2.878	2.149, 2.571	...
0.36	...	...	5.559	2.870	2.230, 2.498	...
0.37	...	...	5.544	2.866	2.298, 2.434	...
0.374	2.374	7.04e^9	5.538	2.865	...	...
0.40	2.435	18.277	5.500	2.854	...	...
0.44	2.540	8.152	5.436	2.837	...	...
0.48	2.645	5.634	5.370	2.820	...	...
0.52	2.753	4.498	5.298	2.801	...	...
8/15	2.789	4.248	5.273	2.795	...	...

(2) The energies corresponding to ISCOs are smaller than those corresponding to larger values of the orbital radii.

(3) It should be observed that for the M-Q$^{(1)}$ solution, there are ISCOs (within $3M$) only for positive values of q (i.e., prolate sources). This important difference between the two cases (prolate and oblate) has been brought out before for the γ [27] and the M-Q$^{(1)}$ [28,62] spacetimes. We ignore what could be (if any) the fundamental physical reason for such a difference.

Finally, Table III displays some values of relevant parameters (mso$_-$, L_- and λ), as well as the interval of nonexistence of stable circular orbits (λ_m, λ_M), for the LM solution with a quadrupole and 2^4-pole.

It should be observed that now, unlike in the case of the M-Q$^{(1)}$ solution, the function $L(\lambda)$ has no maximal value, implying there exists no mso$_+$. Thus, the existence of ISCOs is restricted to the interval $r_s/M \in (0, \lambda_m)$ whenever the quadrupole and the 2^4-pole are localized within the ranges mentioned before Eq. (33).

Also, the value of λ_m is significantly reduced with respect to the M-Q$^{(1)}$ case, and therefore ISCOs are now very close to the infinite-redshift surface ($r_s/M = 2$). At the same time, the range (λ_m, λ_M) increases with respect to the previous case. For values of r_s/M starting from mso$_-$ (the minimum of L), we obtain the values of the farthest possible stable circular orbits.

TABLE III. The case of the LM solution with $g = 2$, i.e., quadrupole and 2^4-pole moments. Numerical values of the multipole parameters q and m_4 for which ISCOs exist. The value of the marginally stable orbit *mso* is given with the corresponding value of the angular momentum parameter L.

q	m_4	mso_-	L_-	(λ_m, λ_M)
−0.063	−0.063	6.000	3.0195	2.000, 3.030
−0.08	−0.08	6.000	3.0248	2.0091, 3.038
−0.10	−0.10	6.000	3.0311	2.0224, 3.047
−0.124	−0.124	6.000	3.0386	2.0385, 3.058
0.0427	−0.0427	5.9501	2.9852	2.000, 2.953
0.05	−0.05	5.9414	2.9826	2.0081, 2.943
0.06	−0.06	5.9294	2.9791	2.024, 2.931
0.07	−0.07	5.9173	2.9756	2.044, 2.917
0.085	−0.085	5.8989	2.9702	2.075, 2.899

IV. CONCLUSIONS

We have presented a systematic study on the structure of circular geodesics in the LM spacetime. The case has been made for the use of such spacetime when describing slight deviations from spherical symmetry.

The analysis presented clearly exhibits the difference between the motion in the Schwarzschild and the LM, spacetimes. In the former case we have a black hole, whereas in the latter a naked singularity appears. Our results, as well as those in the references already mentioned, point to potentially observable evidence alowing us to distinguish between the two above mentioned situations. We may summarize such results as follows:

(1) The presence of multipole moments (higher than the monopole) leads to the presence of ISCOs closer to the infinite-redshift surface than those existing in the exactly spherically symmetric case.
(2) Such multipole moments also produce an interval in the values of radial coordinates within which no stable circular orbits exist.
(3) Specific numerical values have been presented to illustrate the two above mentioned effects.
(4) Particularly relevant might be the application of the presented results to studying the dynamics of accretion discs around compact objects, which as is well known, are assumed to be an essential ingredient of active sources such as x-ray binaries or galactic nuclei (see Ref. [66] and references therein). However, such a study is outside the scope of this paper.

ACKNOWLEDGMENTS

This work was partially supported by the Spanish Ministerio de Ciencia e Innovación under Research Project No. FIS 2012-30926, and the Consejería de Educación of the Junta de Castilla y León under the Research Project Grupo de Excelencia No. GR234.

[1] W. Israel, Phys. Rev. **164**, 1776 (1967).
[2] H. Weyl, Ann. Phys. (Berlin) **54**, 117 (1918).
[3] H. Weyl, Ann. Phys. (Berlin) **364**, 185 (1919).
[4] T. Levi-Civita, Atti. Accad. Naz. Lincei Rend. Classe Sci. Fis. Mat. Nat. **28**, 101 (1919).
[5] J. L. Synge, *Relativity: The General Theory* (North-Holland, Amsterdam, 1960).
[6] H. Stephani *et al.*, *Exact Solutions to Einstein's Field Equations* (Cambridge University Press, Cambridge, England, 2003), 2nd ed.
[7] B. Carter, Phys. Rev. Lett. **26**, 331 (1971).
[8] S. W. Hawking, Phys. Rev. Lett. **26**, 1344 (1971).
[9] R. Wald, Phys. Rev. Lett. **26**, 1653 (1971).
[10] B. Boisseau and P. Letelier, Gen. Relativ. Gravit. **34**, 1077 (2002).
[11] J. Winicour, A. I. Janis, and E. T. Newman, Phys. Rev. **176**, 1507 (1968).
[12] A. Janis, E. T. Newman, and J. Winicour, Phys. Rev. Lett. **20**, 878 (1968).
[13] L. Bel, Gen. Relativ. Gravit. **1**, 337 (1971).
[14] F. I. Cooperstock and G. J. Junevicus, Nuovo Cimento B **16**, 387 (1973).
[15] L. Herrera, Int. J. Mod. Phys. D **17**, 557 (2008).
[16] L. Herrera, Int. J. Mod. Phys. D **17**, 2507 (2008).
[17] R. Bach and H. Weyl, Math. Z. **13**, 134 (1922).
[18] G. Darmois, *Les Equations de la Gravitation Einsteinienne* (Gauthier-Villars, Paris, 1927), p. 36.
[19] D. M. Zipoy, J. Math. Phys. (N.Y.) **7**, 1137 (1966).
[20] R. Gautreau and J. L. Anderson, Phys. Lett. **25A**, 291 (1967).
[21] F. I. Cooperstock and G. J. Junevicus, Int. J. Theor. Phys. **9**, 59 (1974).
[22] B. H. Vorhees, Phys. Rev. D **2**, 2119 (1970).
[23] F. Espósito and L. Witten, Phys. Lett. **58B**, 357 (1975).
[24] K. S. Virbhadra, arXiv:gr-qc/9606004.
[25] J. L. Hernández-Pastora and J. Martín, Gen. Relativ. Gravit. **26**, 877 (1994).
[26] J. L. Hernández-Pastora, J. Martín, and E. Ruiz, Gen. Relativ. Gravit. **30**, 999 (1998).
[27] L. Herrera, F. M. Paiva, and N. O. Santos, Int. J. Mod. Phys. D **9**, 649 (2000).
[28] L. Herrera, Found. Phys. Lett. **18**, 21 (2005).
[29] L. Herrera, A. Di Prisco, and J. Martinez, Astrophys. Space Sci. **277**, 447 (2001).
[30] L. Herrera, A. Di Prisco, and E. Fuenmayor, Classical Quantum Gravity **20**, 1125 (2003).
[31] K. S. Virbhadra, D. Narashima, and S. M. Chitre, Astron. Astrophys. **337**, 1 (1998).

[32] K. S. Virbhadra and G. F. R. Ellis, Phys. Rev. D **65**, 103004 (2002).
[33] K. S. Virbhadra and C. R. Keeton, Phys. Rev. D **77**, 124014 (2008).
[34] G. N. Gyulchev and S. S. Yazadjiev, Phys. Rev. D **78**, 083004 (2008).
[35] C. Bambi and K. Freese, Phys. Rev. D **79**, 043002 (2009).
[36] K. Hioki and K. I. Maeda, Phys. Rev. D **80**, 024042 (2009).
[37] C. Bambi, K. Freese, T. Harada, R. Takahashi, and N. Yoshida, Phys. Rev. D **80**, 104023 (2009).
[38] C. Bambi, T. Harada, R. Takahashi, and N. Yoshida, Phys. Rev. D **81**, 104004 (2010).
[39] Z. Stuchlik and J. Schee, Classical Quantum Gravity **27**, 215017 (2010).
[40] Z. Kovacs and T. Harko, Phys. Rev. D **82**, 124047 (2010).
[41] D. Pugliese, H. Quevedo, and R. Ruffini, Phys. Rev. D **84**, 044030 (2011).
[42] P. Pradhan and P. Majumdar, Phys. Lett. A **375**, 474 (2011).
[43] A. N. Chowdhury, M. Patil, D. Malafarina, and P. S. Joshi, Phys. Rev. D **85**, 104031 (2012).
[44] C. Bambi and G. Lukes-Gerakopoulos, Phys. Rev. D **87**, 083006 (2013).
[45] J. H. Young and C. A. Coulter, Phys. Rev. **184**, 1313 (1969).
[46] D. Bini, C. Cherubini, S. Filippi, and A. Geralico, Gen. Relativ. Gravit. **41**, 2781 (2009).
[47] H. Quevedo and B. Mashhoon, Phys. Lett. **A109**, 13 (1985).
[48] D. Bini, A. Geralico, O. Luongo, and H. Quevedo, Classical Quantum Gravity **26**, 225006 (2009).
[49] V. S. Manko and I. D. Novikov, Classical Quantum Gravity **9**, 2477 (1992).
[50] J. L. Hernández-Pastora, Classical Quantum Gravity **30**, 175003 (2013).
[51] R. Geroch, J. Math. Phys. (N.Y.) **11**, 1955 (1970).
[52] R. Geroch, J. Math. Phys. (N.Y.) **11**, 2580 (1970).
[53] K. S. Thorne, Rev. Mod. Phys. **52**, 299 (1980).
[54] G. Fodor, C. Hoenselaers, and Z. Perjés, J. Math. Phys. (N.Y.) **30**, 2252 (1989).
[55] M. Herberthson, Classical Quantum Gravity **21**, 5121 (2004).
[56] T. Bäckdahl and M. Herberthson, Classical Quantum Gravity **22**, 3585 (2005).
[57] T. Bäckdahl and M. Herberthson, Classical Quantum Gravity **23**, 5997 (2006).
[58] J. L. Hernández-Pastora, Ph.D. thesis, Universidad de Salamanca, 1996.
[59] T. Bäckdahl and M. Herberthson, Classical Quantum Gravity **22**, 1607 (2005).
[60] L. Herrera and J. L. Hernández-Pastora, J. Math. Phys. (N.Y.) **41**, 7544 (2000).
[61] J. L. Hernández-Pastora and J. Ospino, Phys. Rev. D **82**, 104001 (2010).
[62] L. Herrera, J. Carot, N. Bolivar, and E. Lazo, Int. J. Theor. Phys. **48**, 3537 (2009).
[63] L. Herrera, W. Barreto, and J. L. Hernández-Pastora, Gen. Relativ. Gravit. **37**, 873 (2005).
[64] H. Quevedo, Fortschr. Phys. **38**, 733 (1990).
[65] A. F. Teixeira, Prog. Theor. Phys. **60**, 163 (1978).
[66] S. Kato, J. Fukue, and S. Mineshige, *Black-hole Accretion Disks* (Kyoto University Press, Kyoto, 1998).